Hindawi
Journal of Nanomaterials
Volume 2020, Article ID 7140182, 15 pages
https://doi.org/10.1155/2020/7140182

Research Article

Graphene Oxide/Single-Walled Carbon Nanotube Membranes for CO_2 and N_2 Separation from Blast Furnace Gas

Lili Jiang,[1,2] **Yimin Meng**,[2] **Sihao Tu**,[2] **Yuanshou Zhao**,[2] **Qi Cui**,[2] **Wenpeng Zhang**,[2] **Haitao Yu**,[3] **and Xingang Hou**[2]

[1]*State Key Laboratory of Advanced Processing and Recycling of Non-Ferrous Metals, Lanzhou University of Technology, Langongping Road, Lanzhou, 730050 Gansu Province, China*
[2]*School of Material Science and Technology, Lanzhou University of Technology, Langongping Road, Lanzhou, 730050 Gansu Province, China*
[3]*Department of Medical Laboratory, The First Hospital of Lanzhou University, No. 1, Donggang Road, Chengguan District, Lanzhou, 730000 Gansu Province, China*

Correspondence should be addressed to Lili Jiang; jianglili2002@163.com

Received 9 October 2019; Revised 6 December 2019; Accepted 13 January 2020; Published 12 February 2020

Academic Editor: Bhanu P. Singh

A novel molecular sieve membrane was synthesized using graphene oxide/single-walled carbon nanotubes (GO/SWCNTs). The composite was characterized by transmission electron microscopy, field emission scanning electron microscopy, X-ray diffraction, thermogravimetric analysis, Fourier transform infrared spectroscopy, and Brunauer–Emmett–Teller-specific surface area analyzers. The results revealed that laminar GO was interwoven with tubular SWCNTs and the carbon nanotubes were attached onto the surface of GO or interspersed among GO to form a three-dimensional structure. Moreover, the interlayer spacing of GO/SWCNTs increased to 0.826 nm. On condition that the inlet pressure of N_2 was 0.10 MPa and the temperature was 323 K, the N_2 permeability of GO/SWCNTs was 1595 Barrer. With increasing temperature, the N_2 permeability decreased while it increased with the inlet pressure. When the inlet pressure of CO was 0.10 MPa and the temperature was 323 K, the CO permeability was 109 Barrer. At the temperature of 323 K, the selectivities of N_2/CO and CO_2/CO were 32.8 and 37, respectively. These results indicated that GO/SWCNTs may be a promising molecular sieve for gas separation.

1. Introduction

Blast furnace gas (BFG) in iron and steel industry generally has a significant gas yield. The main components of BFG include CO, CO_2, and N_2, in which CO_2 and N_2 are inflammable, causing the utilization rate of BFG to be low and its calorific value is only 3,000 to 3,800 kJ/m^3 [1]. Therefore, the separation of CO_2 and N_2 from BFG in advance can increase the calorific value and improve the utilization rate of BFG, which allows one to reasonably recycle and utilize BFG resources.

As a major method for gas separation, molecular sieve membrane (MSM) is of broad interest [2]. The pore size of MSM approximates the size of a molecule and is of uniform size, so an MSM is extensively used in various aspects including ion exchange and gas separation. At present, the zeolite molecular sieve (ZMS) is the key MSM product [3]. Due the advantages, such as regular open framework, strong acidity, and high hydrothermal stability, ZMS is widely used in various fields including gas separation, adsorption, and ion exchange [4]. However, ZMS also exhibits some disadvantages (including low efficiency, high energy consumption, and serious environmental pollution) in its synthesis, thus posing the severe challenge. Graphene oxide (GO) [5] and carbon nanotubes (CNTs) [6] have promising applications in gas separation due to their favourable adsorption properties, large specific surface area (SSA), low energy consumption, cleanliness, environmentally friendly nature, and high efficiency of gas separation in the synthesis process.

By combining CNTs and GO with a Matrimids matrix, Li et al. [7] prepared mixed matrix membranes (MMMs) to improve the separation performance for CO_2. The selective permeabilities of CNTs and GO show a synergistic effect. CNTs are taken as a channel to lead to a high permeability while GO were used as selective barriers to contribute high selectivity through hydroxyl and carboxyl on the surface of GO. The result showed that the selectivities of CO_2/CH_4 and CO_2/N_2 are 84.60 and 81.00, respectively. Athanasekou et al. [8] prepared a series of independent and GO membranes with a substrate, which are completely permeable to hydrogen (H_2) and helium (He). The result suggested that aluminium oxide-filtering membranes exhibit favourable stability and the He/H_2 selectivity reaches 47.6. Wesolowski and Terzyk [9] explored the gas separation performance of a three-dimensional network structure composed of GO and CNTs. The result obtained through molecular dynamics simulation validated that the material can be used to prepare membranes related to many gas mixtures. Moreover, they explained the potential mechanism of the process. By applying an improved chemical longitudinal melting method, Xue et al. [10] prepared novel multiwalled CNTs (MWCNTs) and GO nanoribbon nanocomposites with a shell structure. Afterwards, the nanocomposites were used as filling materials to strengthen the gas separation performance of polyimide-based MMM. The result showed that, compared with initial polyimide, MMM exhibits higher selectivity for gas and higher gas permeability. The high selectivity for gas can be attributed to the shell of GO nanoribbon, which offers selective barriers and a large zone for gas adsorption. High gas permeability is attributable to hollow-structure MWCNTs with a smooth internal surface, which function as a rapid transmission channel.

By employing a solvent evaporation method, Zhang et al. [11] carbonized GO and polyamide acid (PAA) composite membranes at 600°C to prepare independent-type graphene carbon membranes with a helical structure. On this basis, the permeability of independent-type graphene carbon membranes with different PAA solid contents for CO_2 and CH_4 was investigated. The result indicated that with the increase of PAA solid content, the permeability and ideal selectivity of graphene carbon membranes for CO_2 both improve. The permeation rate of graphene carbon membranes for CO_2 reaches 824 Barrer, and the selectivity of CO_2/CH_4 is 38.9. The channel of graphene carbon membranes for gas permeation is attributed to the layered accumulation of graphene and carbon MS in graphene carbon membranes. The research provides a favourable basis for preparing flexible and independent-type graphene carbon membranes for gas separation. Qiao et al. [12] prepared thin-film nanocomposite (TFN) embedded with GO by using interfacial polymerisation (IP) technology. Furthermore, they explored the influence of GO load on the shape and gas separation performance of membranes. The result revealed that the permeability and selectivity of TFN are positively correlated with the GO content. When the added amount of GO is 0.5 wt.%, the permeation rate of TFN for CO_2 is more than twice that of pure thin-film composite (TFC). Moreover, the CO_2/N_2 and CO_2/CH_4 separation factors of TFN are up to 41 (increasing by 26%) and 25 (increasing by 26%), respectively. The improvement of the performance of TFN is caused by the increased tortuosity of the polymer matrix and the introduction of rapid diffusion channels triggered by the doping of rigid GO lamellae. GO/TFN displays the potential for separating CO_2 [13–16].

The objective of the present study was to synthesize GO/SWCNTs and investigate their separation performance for CO_2 and N_2 from blast furnace gas. The synthesized material was characterized by transmission electron microscopy (TEM), field emission scanning electron microscopy (FESEM), X-ray diffraction (XRD), thermogravimetric analysis (TGA), Fourier transform infrared (FTIR) spectroscopy, and Brunauer–Emmett–Teller (BET) SSA analyzers. Pure and mixed gas experiments were performed. The change in N_2 and CO_2 permeabilities of GO/SWCNTs under different pressures and temperatures was investigated. Additionally, the permeabilities and selectivities of GO/SWCNTs for various components in mixed gas (including N_2, CO_2, and CO) were also observed.

2. Experiments and Methods

2.1. Materials and Reagents. SWCNTs were purchased from Shenzhen Nanotech Port Co., Ltd, (China). According to the manufacturer, the physicochemical properties of SWCNTs are listed in Table 1. Due to the purity being around 90%, SWCNTs should be purified. Natural flake graphite (12,000 mesh) was purchased from Qingdao Tianshengda Graphite Co., Ltd. (China). H_2SO_4, HNO_3, and $KMnO_4$ were purchased from Big Alum Chemical Reagent Factory (China). Ultrapure water was used for the preparation of solution. All of the chemicals were of analytical grade without further purification. N_2, CO_2, and mixed gas (N_2: 60%; CO_2: 20%; and CO: 20%) were purchased from Shanghai Tonghui Special Gas Co., Ltd.

2.2. Characterization Techniques. TEM (type JEM-2010, operating at 200 kV) was used to characterize the morphology of the samples. These samples were dispersed in absolute alcohol by ultrasonic treatment for 15 min. SEM (JSM-6700F, operating at 0.5-30 kV) was applied for observing the surface morphology of materials. An FTIR spectrometer (type Nicotct 5700) was used to analyze the surface functional groups of composite within the 400-4000 cm^{-1} range. TGA was performed on a thermogravimetric analyzer (type NETZSCHSTA-449F3) under an N_2 atmosphere from 40 to 1,200°C at a heating rate of 20°C/min. X-ray diffraction (type D8/AXS, operating at 60 kV) was used to investigate the crystalline phase of the material. A fast SSA analyzer (type ASAP 2010, America Micromeritics Corporation) was applied to analyze the SSA and pore diameter of GO/SWCNTs.

2.3. Preparation of GO/SWCNTs

2.3.1. Preparation of Oxidized SWCNTs. SWCNTs (1 g) were placed in a beaker with 30 mL concentrated sulphuric acid and 10 mL concentrated nitric acid to remove impurities and hemispherical caps. The mixture was then ultrasonically stirred for 24 h. The suspensions were filtered, rinsed with

Table 1: Physicochemical properties of SWCNTs.

Physicochemical property	Value
Diameter	<2 nm
Length	>5 um
Purity	>90%
Ash content	<10%
Specific surface area	600-800 m^2/g

deionized water until the pH reached approximately 7, and dried in a vacuum oven at 80°C for 12 h. The resulting product was the oxidized SWCNTs.

2.3.2. Preparation of GO. GO was prepared using modified Hummers' method [17–19]. Natural graphite (1 g) was dispersed in a three-necked bottle containing 23 mL sulphuric acid below 5°C. The mixture (while below 10°C) was stirred until complete dissolution, followed by slow addition of 0.5 g sodium nitrate and 3 g potassium permanganate, and then the mixture was stirred for 2.5 h. Again, the three-necked bottle was removed and placed in a water bath at 85°C, while being stirred for 24 min and diluted to 560 mL. Then, 10 mL hydrogen peroxide (30 wt.%) was added and kept warm for 5 min where the colour of the mixture became bright yellow. The product was centrifuged and washed with 3% hydrochloric acid for several times to remove residual metal ions until the pH of the product reached 7. Finally, the product was treated by ultrasonication for 1 h, centrifuged, and dried in a vacuum oven for 24 h at 80°C. The resulting product was GO.

2.3.3. Preparation of GO/SWCNTs. 300 mg of GO was placed into a beaker, in which 100 mL of absolute alcohol was added. The mixture was mechanically stirred for 1 h and then ultrasonically processed for 1 h to form a uniform GO dispersion. Afterwards, 10 mg of cetyl trimethyl ammonium bromide (CTAB) was poured into the beaker, where 100 mL of absolute alcohol was added. The mixture was ultrasonicated for 30 min. When the CTAB was completely dispersed in absolute alcohol, 150 mg of purified SWCNTs were added to the beaker, followed by constant ultrasonic treatment for 4 h. Thus, the uniformly dispersed SWCNTs were obtained. The GO dispersion was dropped into the SWCNT dispersion (drop-by-drop) via pipette. Furthermore, the mixture was mechanically stirred for 30 min and then ultrasonically treated for 1 h. The process was repeated three times to produce a stable GO/CNT dispersion. Subsequently, GO/SWCNT dispersion was uniformly dropped into a polytetrafluoroethylene filter membrane (0.45 μm) by applying a pipette for subsequent filtration. It was dried for 24 h in a vacuum drier to acquire the desired GO/SWCNTs. The process of preparation is shown in Figure 1.

2.3.4. Experimental Apparatus for Gas Separation. By using a self-assembled apparatus for gas separation shown in Figure 2, the gas separation performances of MSM synthesized with GO/SWCNTs (hereinafter called GO/SWCNTs MSM) were explored. Based on the pressure difference method [20], the separation performances of GO/SWCNTs MSM for a single gas (CO_2 or N_2) and mixed gas (combinations of CO_2, N_2, and CO) were measured at different experimental temperatures and inlet pressures. The prepared GO/SWCNT MSM was installed in a tube furnace in advance. At first, the experimental system was integrally examined before the experiment to ensure the tightness of the system for gas separation. Afterwards, the tube furnace was turned on to adjust the temperature of the furnace to the corresponding experimental temperature and holding time. Subsequently, the system was subjected to vacuum treatment to guarantee that the system was in a vacuum state. The switch of the gas cylinder was slowly opened. After the reading of pressure gauge had stabilized, the pressure-reducing valve was slowly opened and the reading of the aforementioned pressure (gauge 1) was adjusted to corresponding initial inlet pressure P_0. Next, the flow meter was turned on to adjust its reading to 80 mL/min. After gas was injected, the variation of the reading of pressure gauge 2 above the tube furnace with time was observed. The datum was recorded at a time interval of 5 min until the reading on pressure gauge 2 did not change with time. After the experiment was completed, the switch on the gas cylinder was closed, followed by closing the pressure-reducing valve immediately thereafter. Afterwards, valve 2 was slowly opened and the three-way valve connected to the air storage tank was finally opened to collect the gas at the side for gas permeation. In the process, the pressure-reducing valve was slowly opened to guarantee that the gas between the pressure reducing valve and the switch of air cylinder was emitted. The experiment was ended when the reading on pressure gauge 1 above the pressure-reducing valve was 0.

The permeability and separation factor are important indices used when evaluating the separation performances of MSM [21]. Permeability refers to the permeation rate of gas while the separation factor denotes the relative separation effect after different gases permeate through membranes. The permeability (P) and separation factor (α) were calculated by using Formulas (1), (2), (3), (4), (5), [22]. The permeability of a single gas is expressed by

$$P = \frac{Ql}{A\Delta_P} = \frac{273 \times 10^{10}}{760} \frac{Vl}{AT[P_0 \times (76/14.7)]} \frac{d_p}{d_t}. \quad (1)$$

The permeability of various gas components in mixed gas can be calculated using [23]

$$P_{CO_2} = \frac{y_{CO_2}}{x_{CO_2}} \frac{273 \times 10^{10}}{760} \frac{Vl}{AT[P_0 \times (76/14.7)]} \frac{d_p}{d_t}, \quad (2)$$

$$P_{N_2} = \frac{y_{N_2}}{x_{N_2}} \frac{273 \times 10^{10}}{760} \frac{Vl}{AT[P_0 \times (76/14.7)]} \frac{d_p}{d_t}, \quad (3)$$

$$P_{CO} = \frac{\left(1 - y_{N_2} - y_{CO_2}\right)}{1 - x_{N_2} - x_{CO_2}} \frac{273 \times 10^{10}}{760} \frac{Vl}{AT[P_0 \times (76/14.7)]} \frac{d_p}{d_t}, \quad (4)$$

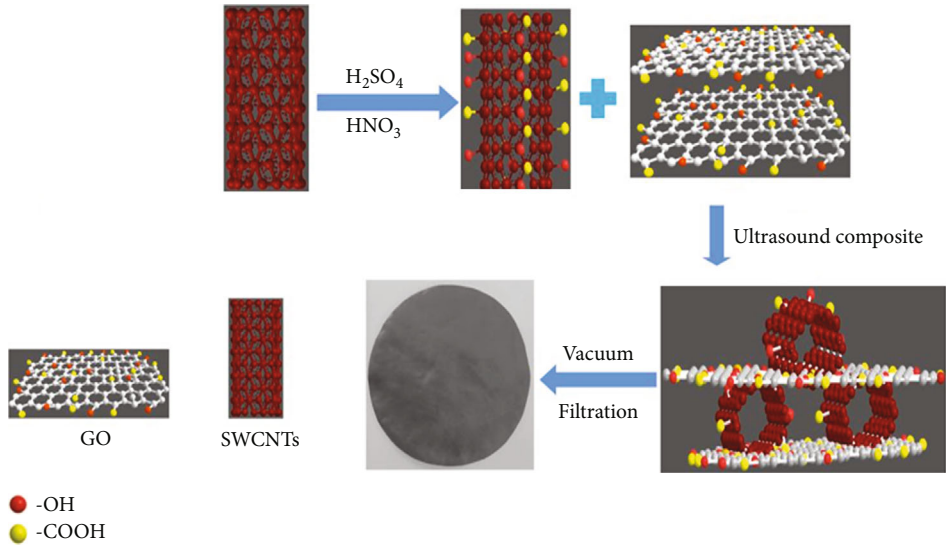

Figure 1: Schematic illustration of GO/SWCNTs.

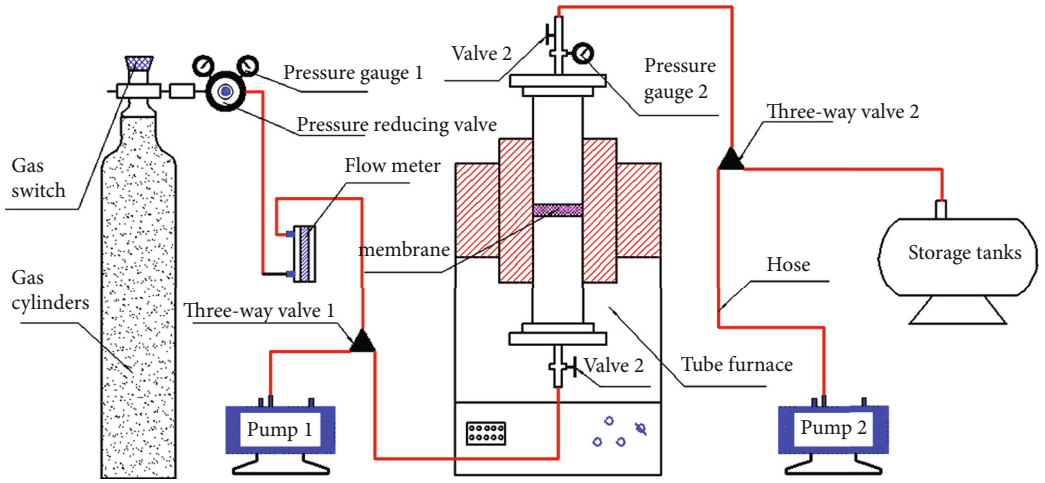

Figure 2: Experimental apparatus for gas separation.

where P refers to permeability (Barrer, where 1 Barrer is equivalent to 1×10^{-10} (STP)·cm·cm^{-2}·s^{-1}·cmHg^{-1}) and Q denotes the permeation flux (J); Δp, V, L, A, T, and P_0 denote the difference in pressures (mm/Hg) at the two sides of MSM, the volume (cm^3) of cavity at the permeation side, the thickness (cm) of MSM, the effective MSM area (cm^2), experimental temperature (K), and initial inlet pressure (psia), respectively. Moreover, x_{N_2} and x_{CO_2} refer to the mole fractions of N_2 and CO_2 at the side of MSM for gas permeation, respectively. Additionally, y_{N_2} and y_{CO_2} represent the mole fractions of N_2 and CO_2 at the air inlet side of MS, respectively; d_p/d_t denotes the increment of the pressure at the side for gas permeation with time.

The true selectivity denotes the separation factor of mixed gas when it passes through a membrane, which can be calculated by using Formula (5) [24]:

$$\alpha_R = \frac{y_A/y_B}{\omega_A/\omega_B}, \quad (5)$$

where ω_A and ω_B refer to the mole fractions of components A and B at the air inlet side of the membrane, respectively; y_A and y_B denote the mole fractions of components A and B at the side for gas permeation of membranes, respectively.

3. Results and Discussion

3.1. TEM. Figure 3 shows the TEM images of the initial SWCNTs, purified SWCNTs, natural graphite, GO, and GO/SWCNTs. As shown in Figure 3(a), the average diameter of SWCNTs was about 10 nm and the initial SWCNTs were interactively crossed, showing slight agglomeration. The end of the initial SWCNTs was smooth and closed. Figure 3(b) shows the TEM image of purified SWCNTs. It can be seen that the length of CNTs treated with mixed acids was shortened: this implied that, after such treatment, the end of each CNT was opened and agglomerations disappeared, generally showing favourable dispersity thereafter. Figure 3(c) shows the TEM image of natural flake graphite

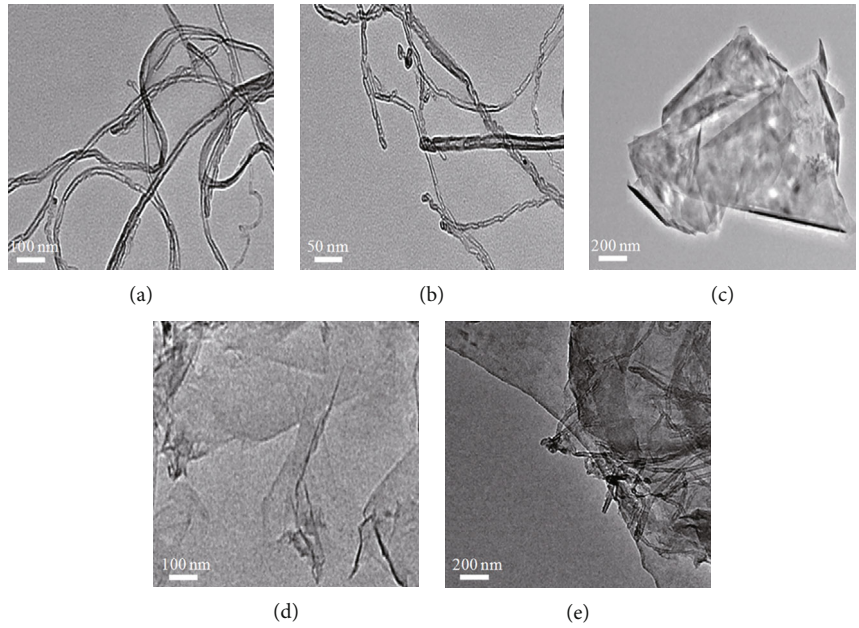

Figure 3: TEM images of (a) SWCNTs, (b) purified SWCNTs, (c) graphite, (d) GO, and (e) GO/SWCNTs.

(12,000 mesh): this exhibited a thick laminar structure, with a width of 2 to 3 μm, which was consistent with claims by manufacturers. Moreover, natural graphite showed even edges and surfaces, and there were many folds on the surface, indicating the accumulation of multilayered graphite lamellae. Figure 3(d) shows a TEM image of GO prepared by modified Hummer's method [13]. According to Figure 3(d), it can be seen that single and few-layer GO lamellae were acquired after natural flake graphite was subjected to oxidation treatment and exfoliated repeatedly using an ultrasonic instrument. Compared with Figure 3(c), the thickness of GO was reduced and the interlayer spacing increased. Some folds remained on the surface of the GO, each measuring about 2 to 3 μm. Figure 3(e) shows a TEM image of GO/SWCNTs: laminar GO and tubular CNTs were interwoven to form composites. CNTs were attached to the surface of GO or interspersed between GO lamellae to form a spatial stereostructure. The stereostructure provided sufficient channels for gas flow through GO/SWCNTs, and therefore, the gas permeability was increased.

3.2. SEM. Figure 4 displays the SEM images of initial SWCNTs, purified SWCNTs, natural flake graphite, GO, and GO/SWCNTs. According to Figure 4(a), it can be seen that the length and diameter of the initial SWCNTs were about 2 to 5 μm and 10 nm, respectively. The CNTs were interactively crossed to cause significant agglomeration. Moreover, the end of the tube wall was smooth and closed, so the dispersity of CNTs cannot be improved unless they were purified. Figure 4(b) shows the SWCNTs purified by using mixed acids: the agglomeration of CNTs was significantly alleviated, having a favourable dispersity. The surface of CNTs oxidized using mixed acids was uneven and exhibited many grooves. The length of CNTs decreased, and the ends of a large number of CNTs with lengths between 100 and 300 nm were all opened; moreover, catalysts and impurities on tube walls disappeared. Figures 4(c) and 4(d) separately present the SEM images of graphite and GO. According to Figure 4(c), it can be seen that natural flake graphite, with a diameter of 2 to 3 μm, was laminar, with a smooth surface. Several laminar graphite structures were accumulated, and the graphite lamellae were tightly pressed with a low interlayer spacing. The graphite lamellae of GO prepared by applying improved Hummer's method were separated after multiple oxidation treatments and exfoliation by ultrasonic instrument, and thus, the interlayer increased. It can be seen from the tilted edge of the GO that each GO had a single layer, or multiple layers, and the thickness of GO lamellae decreased while remaining in the form of irregular polygons. According to Figures 4(e) and 4(f), the laminar GO was interactively interwoven with tubular CNTs and parts of the CNTs were inserted into the GO lamellae to form a spatial stereostructure. GO exhibited a favourable support effect as a framework. Additionally, a part of the CNTs was attached onto the surface of GO through π-π bonds. The result validated the successful synthesis of GO/SWCNTs [25]. The spatial stereostructure provides sufficient nanosized channels for gas to flow through GO/SWCNTs, and therefore, GO/SWCNTs function as an MSM.

3.3. XRD. XRD is the most widely used technique to characterize the crystalline phase of synthesized materials. Figure 5 shows the XRD pattern of graphite, GO, SWCNTs, and GO/SWCNTs. Figure 5(a) shows a characteristic peak at a diffraction angle 2θ of 26.8°, which corresponded to the (002) crystal face of natural graphite, with a favourable crystallinity. According to the Bragg equation ($2d \sin\theta = n\lambda$) [26], the interlayer spacing of natural flake graphite was about 0.332 nm. Figure 5(b) shows the XRD pattern of GO: after natural flake graphite was oxidized (using an oxidant), a characteristic diffraction peak of GO appeared at

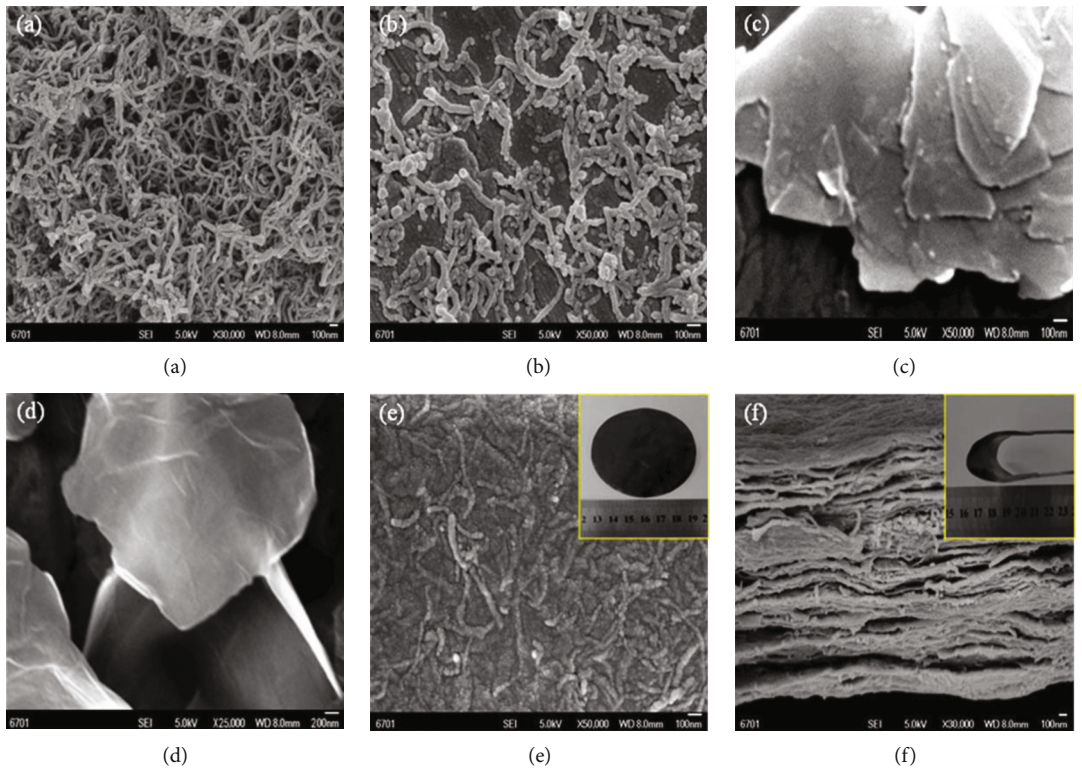

Figure 4: SEM images of (a) SWCNTs, (b) purified SWCNTs, (c) graphite, (d) GO, and (e) and (f) GO/SWCNTs.

$2\theta = 21.63^{\circ}$. Compared with that of the (002) crystal face of natural graphite, the characteristic peak had shifted and its intensity was significantly reduced, showing the poor crystallinity. Through calculation, the interlayer spacing of GO was 0.743 nm. The reason was that, when preparing GO, a great number of oxygen-containing groups (such as hydroxyl (-OH) and carboxyl (-COOH)) were interspersed between graphite lamellae: as a result, the interlayer spacing of GO increased [27]. Additionally, exfoliation using an ultrasonic instrument contributed to improving the interlayer spacing of GO. The XRD pattern of SWCNTs (Figure 5(c)) showed that there was a sharp peak, which was corresponding to the perfect structure of graphite. Although SWCNTs was treated by mixed acid, it remained the perfect structure. The diffraction peak of GO/SWCNTs indicated that, although being subjected to treatment using strong acids and ultrasonication, the (002) crystal face remained in the graphite structure, implying the intact graphite structure in GO and CNTs (Figure 5(d)). However, the range of peak intensity was widened, which indicated that the crystallinity decreased and the size of the graphite structural unit increased. Additionally, due to the addition of SWCNTs, the characteristic peak of GO was left-shifted to $2\theta = 10.7^{\circ}$. Through calculation, it can be seen that the interlayer spacing of GO increased to 0.826 nm because many SWCNTs were inserted into GO to further increase the interlayer spacing of GO [28]. Therefore, it can be judged that GO and SWCNTs were not simply physically mixed while GO was connected with SWCNTs under the effect of Van der Waals force or chemical bonds.

3.4. FTIR. FTIR spectra were a standard method used for the characterization of functionalized material. Figure 6 shows the FTIR spectra of SWCNTs, GO, and GO/SWCNTs: there was a strong characteristic peak at 1570 cm^{-1}, belonging to the C=C vibration peak of SWCNTs (Figure 6(a)) and GO (Figure 6(b)). It validated that the sp2 hybridized structure in the composites was not damaged. The bands at 1090 cm^{-1} and 3440 cm^{-1} were ascribed to O-H stretching vibration [29]. Due to SWCNTs being treated by the mixed acid, there were oxygen-containing groups (-OH) on the surface of SWCNTs (Figure6(a)). Figure 6(b) reveals that -OH and C=O appeared on the surface of GO. Figure 6(c) shows C=O vibration band at 1710 cm^{-1} was found, which corresponded to carboxyl in GO/SWCNTs. The oxidizing treatment produced hydroxy and carboxyl groups on the outermost surface and defect sites that increased the hydrophilicity of SWCNTs. The band at 2800-3000 cm^{-1} was associated with symmetric and asymmetric $-CH_2$ stretching vibration (Figure 6(c)). The aforementioned results indicate that oxygen-containing groups were loaded onto the surfaces of the SWCNTs and GO to allow successful synthesis of composite GO/SWCNTs.

3.5. TGA. TGA was conducted to quantify the mass fraction of the functional groups on the surface of the composite materials. Figure 7 shows the TGA curve of GO, SWCNTs, and GO/SWCNTs. Figure 7(a) showed that from 36°C to 215.98°C, mass loss was about 45.02%, which is because of the decomposition of the -COOH and OH groups and absorbed water. Besides, the mass loss is 29.22%, which may be the decomposition of GO from 215.98°C to

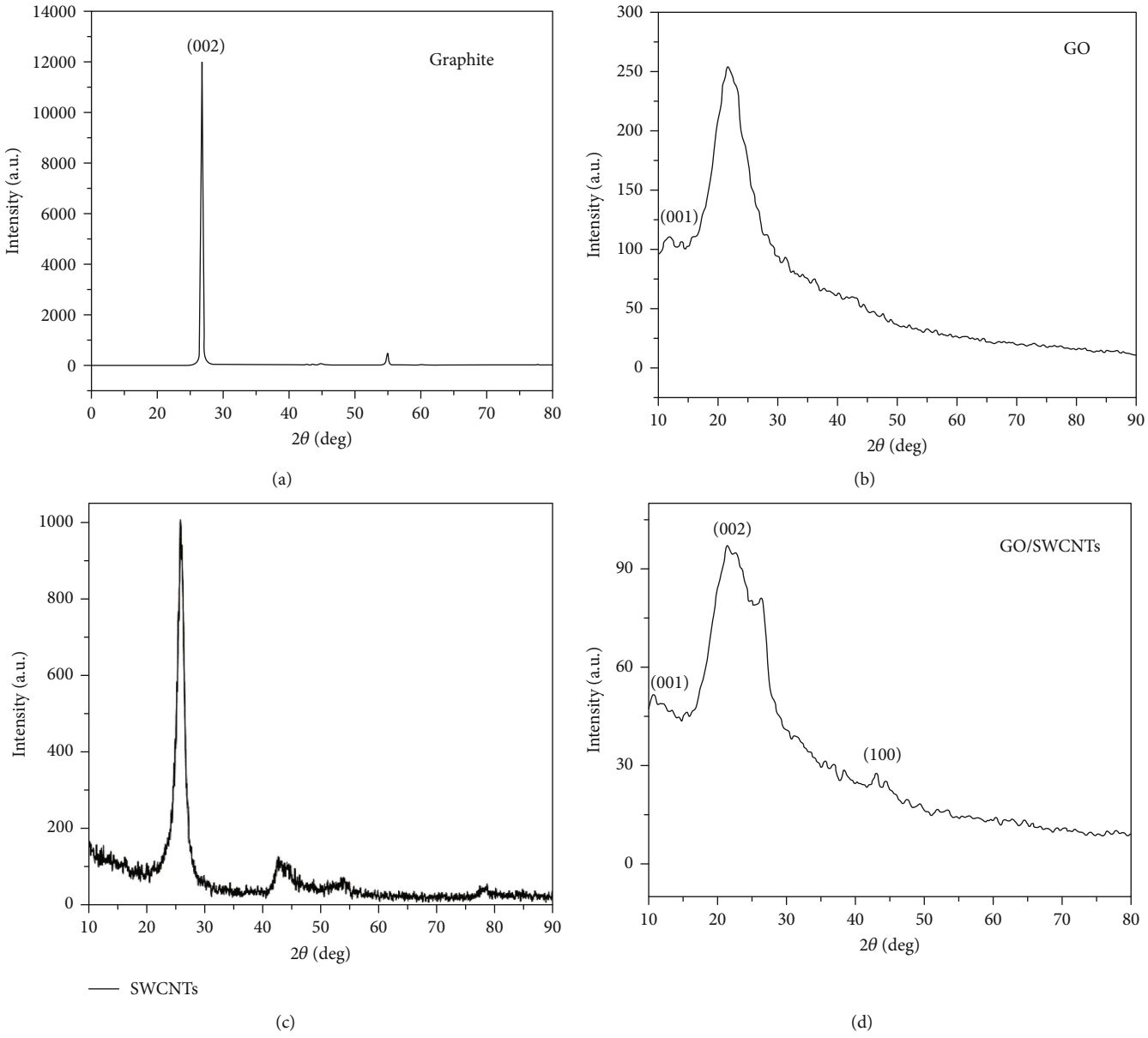

Figure 5: XRD pattern of (a) graphite, (b) GO, (c) SWCNTs, and (d) GO/SWCNTs.

985.06°C. Figure 7(b) shows weight loss was 11.57 wt.% from 94°C to 1156°C, which was due to the decomposition of groups (-COOH and OH) on the surface of oxidized SWCNTs. Figure 7(c) indicates that the curve of GO/SWCNTs was mainly divided into three stages: in the first stage, mass loss was found at temperatures between19.55°C and 162.05°C (5.50 wt.%). The reason was that water between GO lamellae or being adsorbed onto CNTs was evaporated or residual absolute alcohol was volatilized; in the second stage, mass loss appeared in the temperature range from 162.05°C to 255.05°C, during which the mass loss reached 7.15 wt.%. This was mainly caused by the decomposition of hydroxyl and carboxyl (oxygen-containing functional groups) in GO/SWCNTs [30]; in the third stage, the mass loss occurred at temperatures ranging from 255.05°C to 500°C and reached 8.94 wt.%. The reason for this was that amorphous carbon in GO/SWCNTs decomposed. After the temperature rose to 500°C, the mass fraction of GO/SWCNTs remained unchanged, which indicated that the graphite structure of GO and CNTs in GO/SWCNTs was not damaged, with a residual mass fraction of about 79.57%.

3.6. BET. Figure 8 shows the N_2 adsorption-desorption isotherm, pore size distribution, and SSA of GO/SWCNTs samples: various parameters (such as pore size and SSA) of samples can be acquired. As shown in Figure 8(a), at a low relative pressure, the adsorption of GO/SWCNTs composite for N_2 slowly rose and the N_2 adsorption isotherm was a V-shaped curve with hysteresis loops. Therefore, it can be found that the composite was mesoporous and the adsorption isotherm was not consistent with the desorption isotherm, which appeared as a loop structure (type-A loop). This

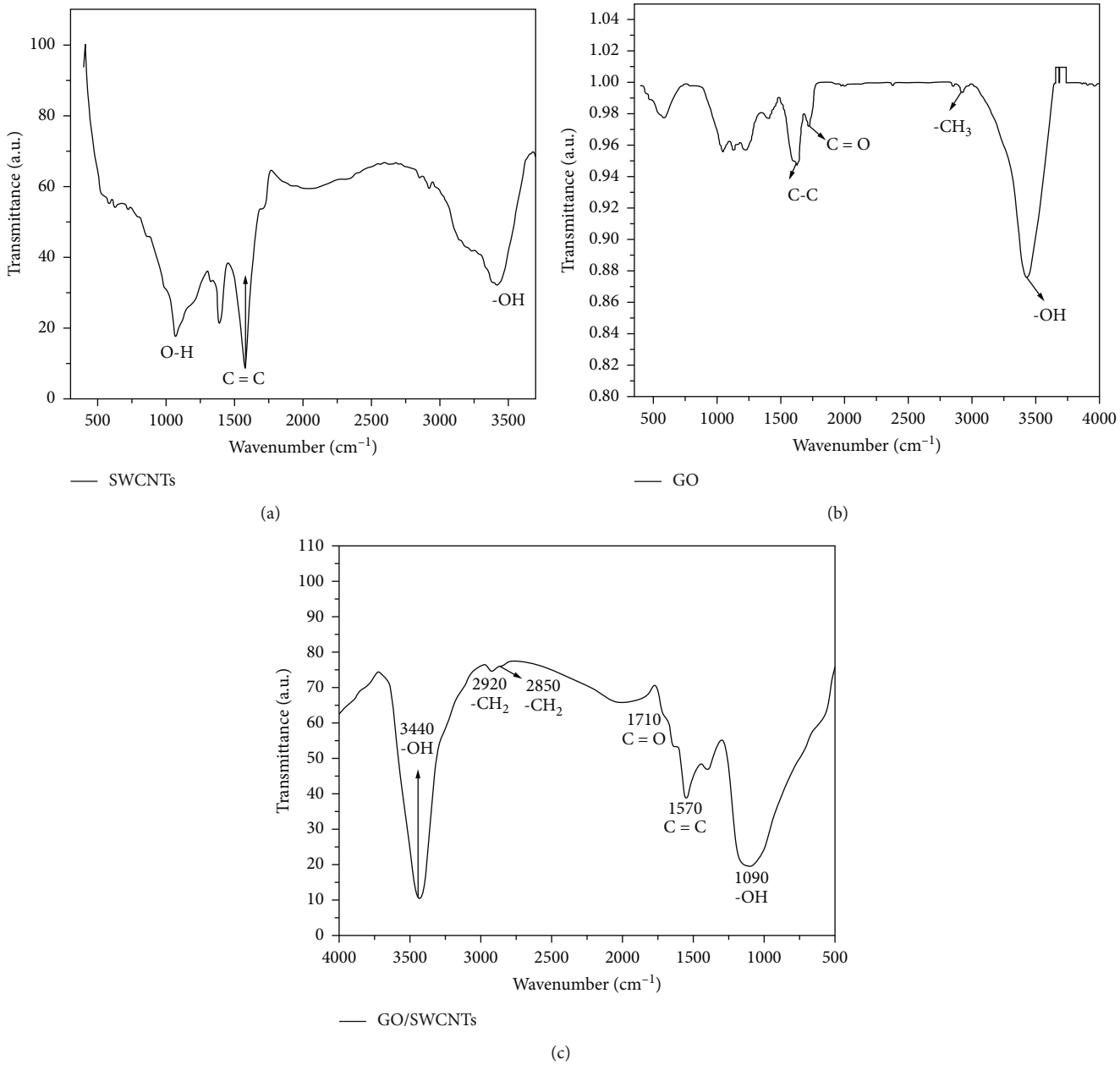

Figure 6: FTIR spectra of (a) SWCNTs, (b) GO, and (c) GO/SWCNTs.

validated the idea that the composite material contained open cylindrical pores. As shown in Figure 8(b), the pore size of samples calculated through the use of the BJH method was mainly distributed in the range of 5 to 13 nm, further validating that the GO/SWCNT composite materials were mesoporous. Figure 8(c) shows the SSA of materials calculated by using the BET equation. Through calculation, the SSA of this GO/SWCNT composite material was 235.79 m^2/g; however, the measured value was much lower than the theoretical value, possibly because of the incomplete exfoliation of GO, having no gap in the GO, and agglomeration of SWCNTs [31].

3.7. Separation Performance of GO/SWCNTs for a Single Gas. Figure 9 shows the N_2 and CO_2 permeability of GO/SWCNTs under different pressures and temperatures. The error bars also are shown in Figure 9. Data were measured for three times. Figure 9(a) indicates that, at an inlet pressure of N_2 of 0.10 MPa, the N_2 permeability was 1595 Barrer at 323 K. As the temperature rose, the N_2 permeability decreased. At 473 K, the N_2 permeability decreased to 1294 Barrer. With increasing inlet pressure, the N_2 permeability increased. At an inlet pressure of 0.15 MPa, the N_2 permeability was 1753 Barrer at 323 K: this indicated that increasing the inlet pressure of gas was conducive to gas flow through the MSM as driven by a high difference in concentrations across the two sides of the MSM. With increasing temperature, the N_2 permeability showed a similar trend (gradually reducing); however, although the N_2 permeability decreased, it was still higher than that at an inlet pressure of 0.10 MPa. When the inlet pressure increased to 0.20 MPa and the temperature

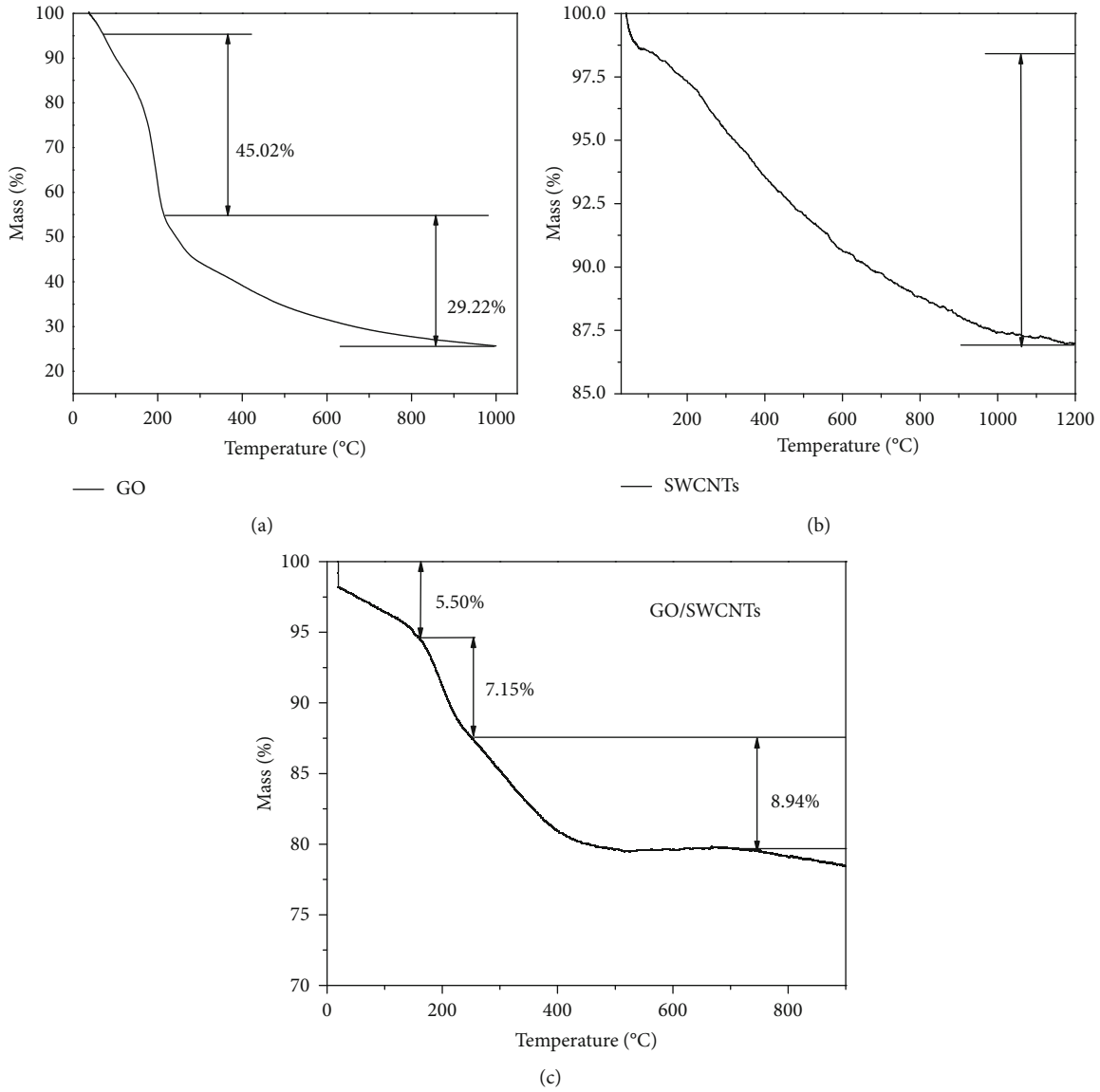

Figure 7: TGA curve of (a) GO, (b) SWCNTs, and (c) GO/SWCNTs.

was 323 K, the N_2 permeability (1883 Barrer) was the highest. The result indicated that, with increasing inlet pressure, the N_2 permeability rose while it decreased with increasing temperature and this was possibly caused by Knudsen diffusion [32]. On condition that the pore size of MSM was lower than the average free path of gas molecules, the collision between gas molecules and pore walls was more common than that between molecules. In this context, Knudsen diffusion occurred; therefore, with increasing temperature, the average free path of gas molecules increased, thus leading to the reduction of the permeability; however, with increasing inlet pressure, the N_2 permeability increased because the rate of Knudsen diffusion was positively proportional to the pressure difference at a certain temperature, thus resulting in an increased permeability.

When the inlet pressure was around 0.2 MPa, the growth in the permeability decreased slightly because of surface diffusion. The gas molecules were chemically reacted with the surface of MSM, and therefore, they were adsorbed onto the surface layer of the membranes. The gas molecules adsorbed onto the pore wall were diffused to the surface due to the difference of concentrations in an adsorption state [33]. Surface diffusion was not related to the relative molecular mass of separated gas molecules. At a certain pressure difference, the rate of chemical adsorption increased with the temperature, so surface diffusion played the dominant role. Additionally, the average free path of gas molecules grew to lead to the reduction of the Knudsen diffusion rate. At a certain temperature, the rate of surface diffusion rose at first and then stabilized with an increasing pressure difference between the two sides of the MSM. On the other hand, the permeation rate for gas was also related to the solubility coefficient [34] and diffusion coefficient of gas. The solubility coefficient of the gas decreased with increasing temperature

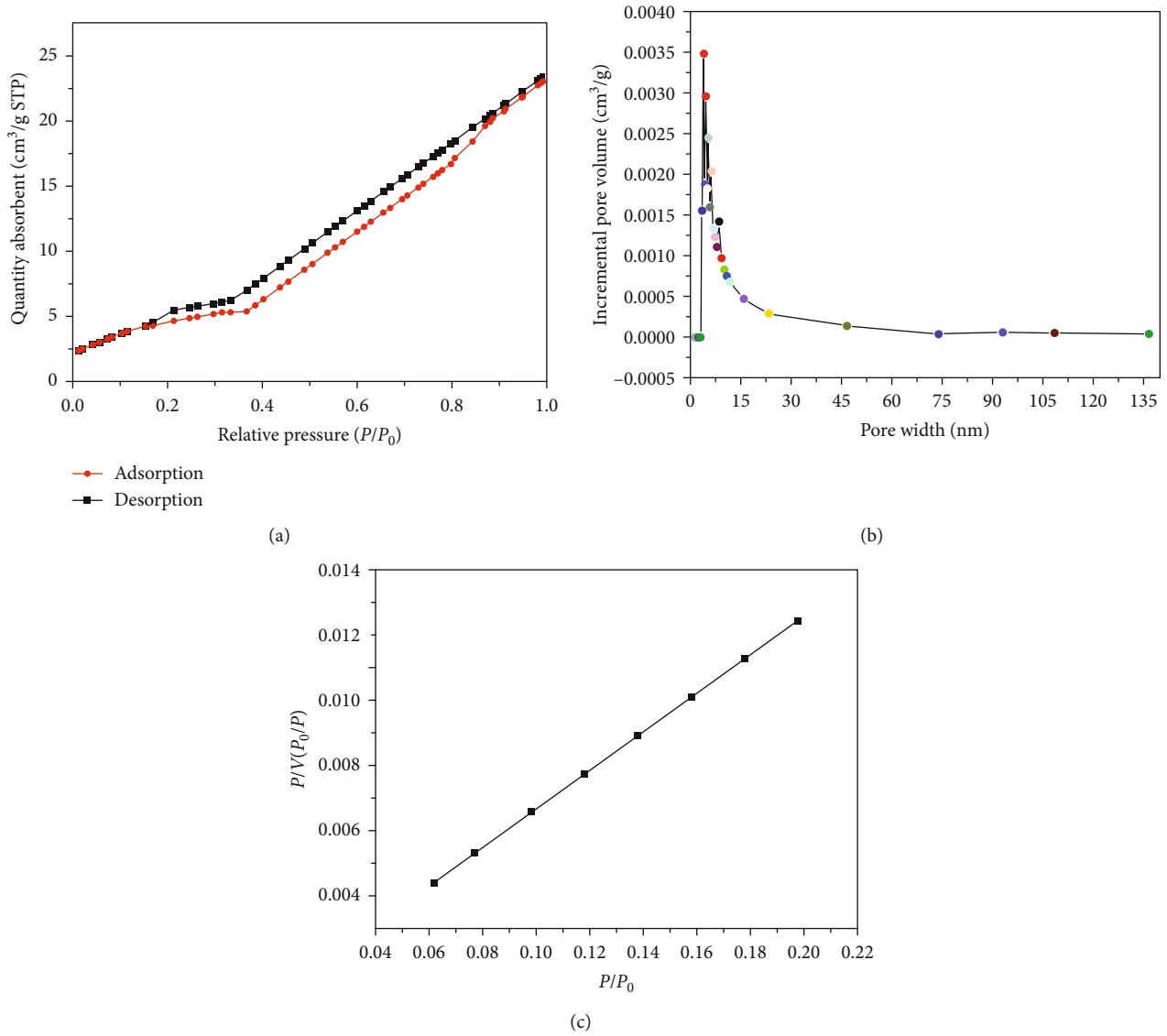

FIGURE 8: N_2 adsorption-desorption isotherm (a); pore size distribution (b); SSA of GO/SWCNTs (c).

and increased with the pressure at a certain temperature; therefore, the rate of permeation decreased with increasing temperature while increasing with the inlet pressure.

Figure 9(b) shows the CO_2 permeability of GO/SWCNTs under different pressures and temperatures. When the inlet pressure was 0.10 MPa and the temperature was 323 K, the CO_2 permeability was 1632 Barrer compared to the N_2 permeability of 1595 Barrer: this indicated that CO_2 preferentially passed through GO/SWCNTs, which functioned as an MSM. The reason was that the molecular dynamics diameters of N_2 and CO_2 were 0.364 and 0.33 nm, respectively, and therefore, the diffusion of N_2 was restricted by the channel. The gas with a larger molecule was constrained outside the channel while that with a smaller molecule preferentially passed through the channel of the MSM. As the temperature increased, the CO_2 permeability gradually decreased, matching the trend in N_2 permeability. With increasing inlet pressure, the CO_2 permeability gradually increased. Especially, in the case that the inlet pressure increased to 0.2 MPa, the CO_2 permeability reached 1900 Barrer at 323 K while it decreased to 1580 Barrer at 473 K.

3.8. The Separation Performance of GO/SWCNTs for Mixed Gas. BFG is a colourless, tasteless, toxic gas fuel with a low calorific value [35], whose main components are listed in Table 2: the main reason why BFG has low recovery is that there are high contents of inert gas (including CO_2 and N_2) in BFG. Therefore, the influence of GO/SWCNTs on the permeability and selectivity of various components in mixed gas (including N_2, CO_2, and CO) was experimentally explored. Figure 10 shows the permeabilities of various gas components in mixed gas (including N_2, CO_2, and CO) under different pressures and temperatures. The error bars also are shown in Figure 10. Data were measured for three times. Figure 10(a) shows that, at an inlet pressure of N_2 of 0.10 MPa, the N_2 permeability was 1637 Barrer at 323 K.

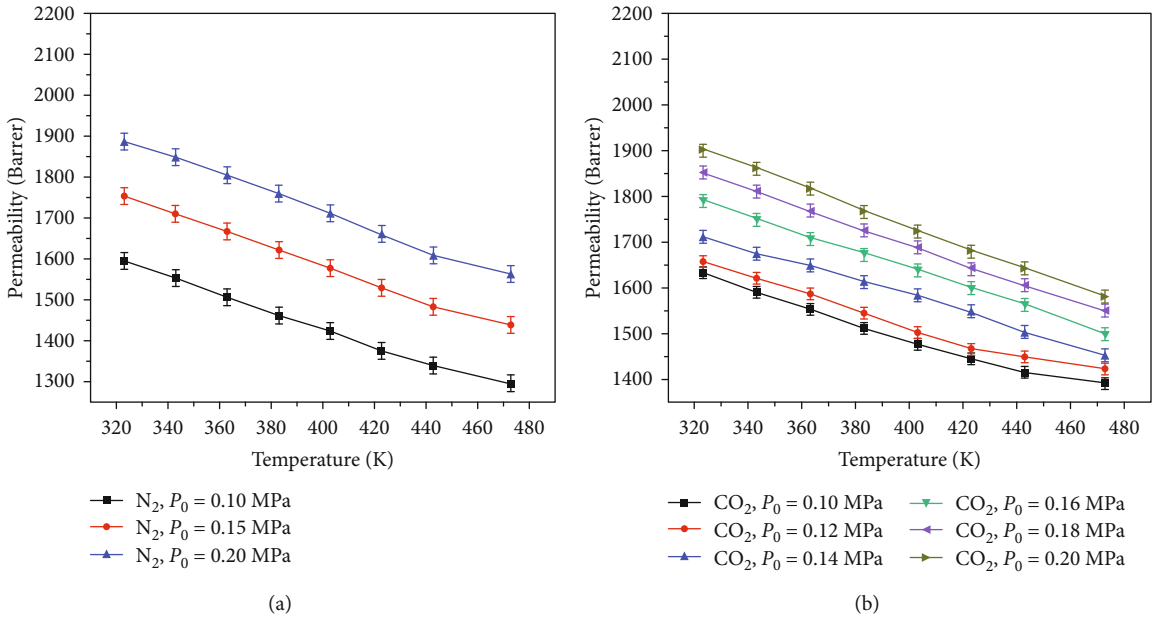

Figure 9: The permeabilities of GO/SWCNTs for a single gas (N_2 (a) and CO_2 (b)) under different pressures and temperatures.

Table 2: Components of BFG.

Main component	CO	CO_2	N_2	CH_4	H_2	Sulphide
wt.%	22~27	13~19	54~58	0.2~0.4	1~4	Trace

With increasing temperature, the N_2 permeability decreased. At 473 K, the N_2 permeability decreased to 1342 Barrer. At an inlet of 0.20 MPa, the N_2 permeability was 1897 Barrer at 323 K, implying that increasing the inlet pressure increased the pressure difference across the GO/SWCNTs, which was conducive to the flow of N_2 through the MSM. At 473 K, the N_2 permeability was 1563 Barrer. The trend matched that of the permeability of a single gas, indicating that the other gases (including CO_2 and CO) in mixed gas did not significantly influence the N_2 permeability and N_2 still passed through the GO/SWCNTs.

Figure 10(b) shows that, at an inlet pressure of CO_2 of 0.20 MPa, the CO_2 permeability was 1976 Barrer at 323 K while it decreased to 1685 Barrer at 473 K. The result showed that although the other gas components in the mixed gas competed with CO_2 in permeation terms, the CO_2 permeability remained large. CO_2 and N_2 preferentially went through GO/SWCNTs, which functioned as an MSM. Figure 10(c) indicates that the CO permeability was low in GO/SWCNTs. At an inlet pressure of CO of 0.10 MPa, the CO permeability was 109 Barrer at 323 K. At 473 K, the CO permeability was 88 Barrer. As the inlet pressure increased to 0.20 MPa, the CO permeability was 149 Barrer at 323 K and it reduced to 124 Barrer at 473 K. A low CO permeability implied that GO/SWCNTs allowed CO_2 and N_2 to preferentially go through while preventing CO from going through when mixed gases passed through GO/SWCNTs; therefore, GO/SWCNTs served as an MSM. One of the purposes of the experiment was to separate CO_2 and N_2 with a low calorific value from BFG. The GO/SWCNTs prepared in the experiment can be used to separate gas. The maximum N_2 permeability in mixed gas was 1897 Barrer while that for CO_2 reached 1976 Barrer. By contrast, the CO permeability was, at most, 149 Barrer. It can be seen that, in terms of the permeabilities of various gas components in mixed gas under the same experimental temperature and inlet pressure, various gas components were, in a descending order, CO_2, N_2, and then CO. The CO permeability was the lowest, only ranging from dozens to hundreds of Barrer. The CO_2, N_2, and CO permeabilities varied, which was likely caused by the synergistic effect between Knudsen diffusion and surface diffusion. Owing to CO_2 and N_2 having a low diameter and strong adsorption capacity, the permeabilities for the two gases were far larger than that for CO. Additionally, when separating mixed gas, the permeabilities of various gas components were all related to the diffusion capacity, competitive adsorption capacity, and their synergistic effect of various gas components [36].

Figure 11 shows the separation selectivity of various gas components in mixed gas (including N_2, CO_2, and CO) at an inlet pressure of 0.1 MPa at different temperatures. As shown in Figure 11(a), the N_2 permeability was 1637 Barrer at 323 K while it was 1342 Barrer at 473 K. The CO permeability also exhibited a similar trend with increasing temperature. The selectivity of N_2/CO slightly increased with increasing temperature. At 323 K, the selectivity of N_2/CO was 32.8, indicating that N_2 preferentially passed through the channels of the MSM when the mixed gas passed through GO/SWCNTs. It was also correlated with the molecular dynamics-based diameter of the gas molecules. The molecular dynamics diameter of N_2 was 0.364 nm, which was slightly lower than that (0.376 nm) of CO. The uniform nanosized channel in GO/SWCNTs prevented CO with a large diameter from going through while allowed N_2 to pass. Additionally, a high selectivity also revealed that GO/SWCNTs functioned as an MSM, which can efficiently

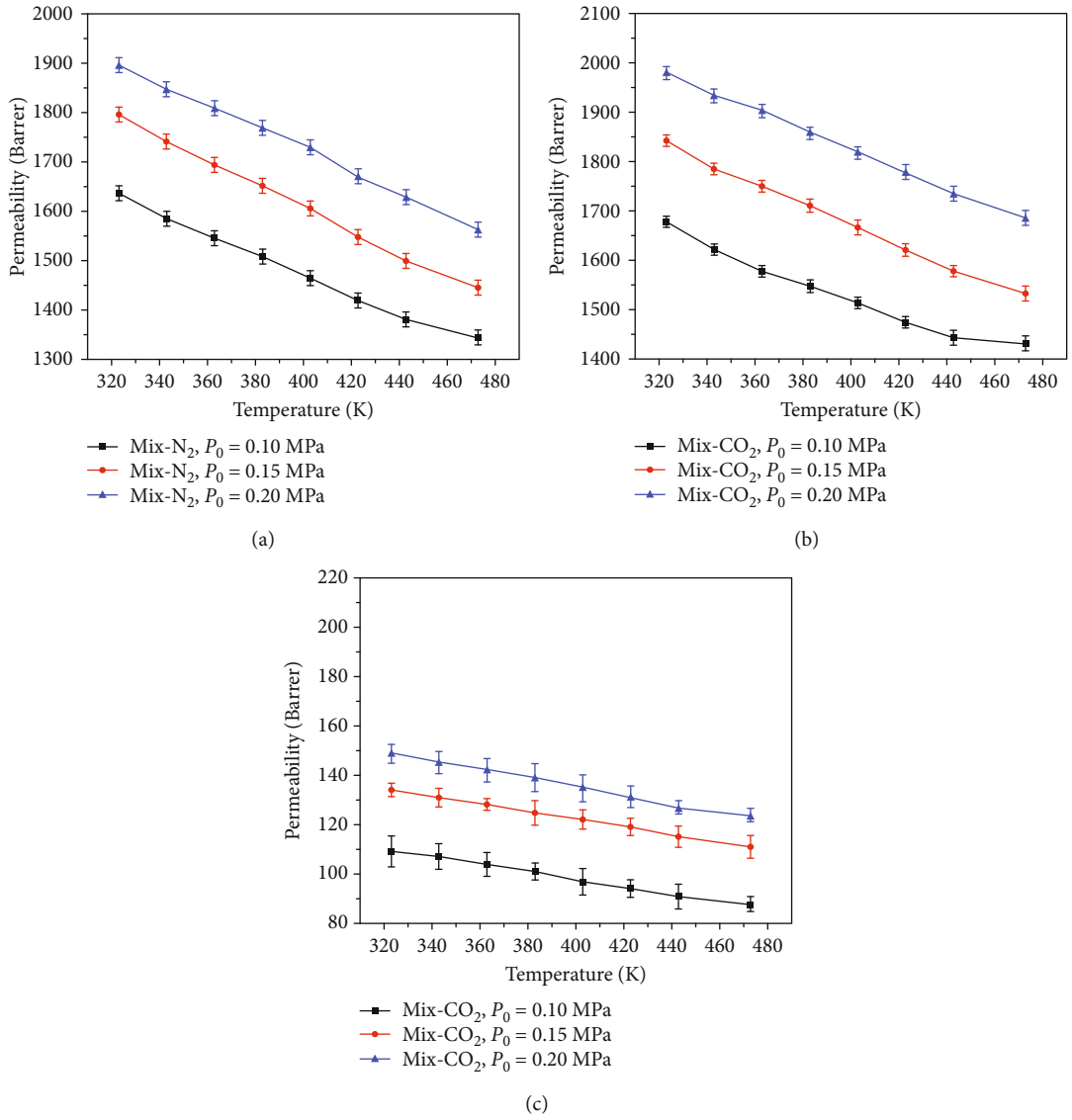

Figure 10: Permeabilities of various gas components in mixed gas (including N_2 (a), CO_2 (b), and CO (c)) under different pressures and temperatures.

separate N_2 and CO from mixed gas. Figure 11(b) shows that the CO_2 permeability was much greater than that for CO. With increasing temperature, the permeabilities of the two gases both slightly decreased while their selectivity did not change to any significant extent. Such high separation selectivity implied that the MSM synthesized with GO/SWCNTs successfully separated N_2 and CO_2 from mixed gas and exhibited the optimal separation performance for CO_2, followed by N_2. In Figure 11(c), the N_2 permeability approximated to that for CO_2 and temperature exerted an insignificant influence on the N_2 permeability. Additionally, the maximum separation selectivity of CO_2/N_2 was 8.3, which did not vary significantly with increasing temperature. Although the separation selectivity of CO_2/N_2 was low, the permeabilities of the two gases were high. It revealed that the MSM exhibited favourable permeabilities to CO_2 and N_2 while the separation selectivities of the two gases were relatively low. The difference in separation selectivity was possibly caused by diffusion separation. CO_2 and N_2 exhibited approximate molecular dynamics diameters; however, the minor difference triggered a significant change in the diffusion coefficient of gas in the channels of the MSM, thus realizing gas separation. The excellent separation performance was attributed to regular nanosized channels and even the material structure in GO/SWCNTs MSM; however, it did not affect the separation of CO_2 and N_2 from mixed gas (including CO_2, N_2, and CO). The reason was that the separation factors of N_2/CO and CO_2/CO in mixed gas separately reached 32.8 and 37, showing high separation selectivity.

4. Conclusions

GO/SWCNTs were successfully prepared and used for the separation of CO_2 and N_2 from BFG. TEM results show that laminar GO was interwoven with tubular SWCNTs and CNTs were attached to the surface of GO or interspersed

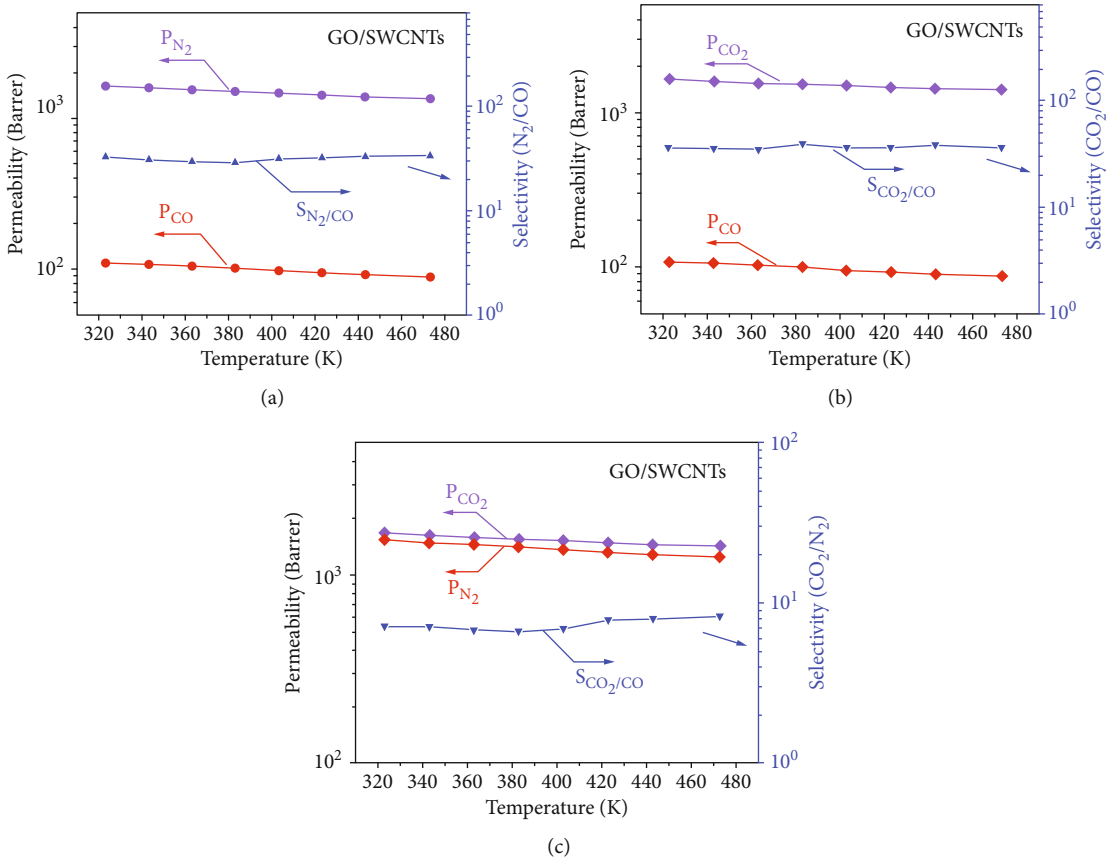

Figure 11: Separation selectivities (including N_2/CO (a), CO_2/CO (b), and CO_2/N_2 (c)) of various gas components in mixed gas at different temperatures at *s*.

between lamellae of GO to form a spatial stereostructure. The structure provided sufficient channels for gas flow through GO/SWCNTs. The interlayer spacing of GO/SWCNTs increased to 0.826 nm because many SWCNTs were inserted into the lamellae of GO. At an inlet pressure of N_2 of 0.10 MPa, the N_2 permeability of GO/SWCNTs was 1595 Barrer at 323 K. The N_2 permeability significantly decreased with increasing temperature while increasing with the inlet pressure. The CO_2 permeability of GO/SWCNTs exhibited a similar trend. The experiment separating CO_2 and N_2 from BFG (including CO_2, N_2, and CO) through GO/SWCNTs showed that the CO permeability was 109 Barrer when the inlet pressure of CO was 0.10 MPa at 323 K. It indicated that when mixed gas went through GO/SWCNTs, GO/SWCNTs allowed CO_2 and N_2 to preferentially pass while preventing CO from doing so; thus, GO/SWCNTs exhibited the functional behaviour of an MSM. At 323 K, the selectivity of N_2/CO was 32.8 while that of CO_2/CO was 37. Such high selectivity indicated that GO/SWCNTs can be used to separate CO_2 and N_2 from BFG.

Data Availability

All the data supporting the results are shown in the paper and can be applicable from the corresponding author.

Conflicts of Interest

The authors declare that there are no competing interests regarding the publication of this paper.

Acknowledgments

The authors are grateful for the financial support from the National Natural Science Foundation of China (51764039); Basic Public Welfare Research Project of Zhejiang Province (LQ19E040006); State Key Laboratory of Advanced Processing and Recycling of Non-Ferrous Metals, Lanzhou University of Technology (SKLAB02019013); and Doctor Research Foundation of Lanzhou University of Technology (061702); GanSu Province Key Research and Development Plan; and Project of Hongliu Support Discipline of Lanzhou University of Technology.

References

[1] B. Kraftschik, W. J. Koros, J. R. Johnson, and O. Karvan, "Dense film polyimide membranes for aggressive sour gas feed separations," *Journal of Membrane Science*, vol. 428, pp. 608–619, 2013.

[2] L. Jiang, H. Yu, L. Pei et al., "Initial concentrations of adsorbate influence on synergistic effect between a magnetic field and graphene oxide-carbon nanotube composite for Pb^{2+} and

phenol adsorption," *Desalination and Water Treatment*, vol. 133, pp. 92–102, 2018.

[3] Y.-J. Fu, K.-S. Liao, C.-C. Hu, K.-R. Lee, and J.-Y. Lai, "Development and characterization of micropores in carbon molecular sieve membrane for gas separation," *Microporous and Mesoporous Materials*, vol. 143, no. 1, pp. 78–86, 2011.

[4] J. N. Yan, H. Y. Gao, Y. G. Zhang, and R. Li, "Research on formation and gas separation performance of polyetherimide based carbon molecular sieve membranes," *Journal of Functional Materials*, vol. 43, no. 4, pp. 469–472, 2012.

[5] K. S. Novoselov, "Electric field effect in atomically thin carbon films," *Science*, vol. 306, no. 5696, pp. 666–669, 2004.

[6] S. Iijima, "Helical microtubules of graphitic carbon," *Nature*, vol. 354, no. 6348, pp. 56–58, 1991.

[7] X. Li, L. Ma, H. Zhang et al., "Synergistic effect of combining carbon nanotubes and graphene oxide in mixed matrix membranes for efficient CO_2 separation," *Journal of Membrane Science*, vol. 479, pp. 1–10, 2015.

[8] C. Athanasekou, M. Pedrosa, T. Tsoufis et al., "Comparison of self-standing and supported graphene oxide membranes prepared by simple filtration: gas and vapor separation, pore structure and stability," *Journal of Membrane Science*, vol. 522, pp. 303–315, 2017.

[9] R. P. Wesolowski and A. P. Terzyk, "Pillared graphene as a gas separation membrane," *Physical Chemistry Chemical Physics*, vol. 13, no. 38, pp. 17027–17029, 2011.

[10] Q. Xue, X. Pan, X. Li, J. Zhang, and Q. Guo, "Effective enhancement of gas separation performance in mixed matrix membranes using core/shell structured multi-walled carbon nanotube/graphene oxide nanoribbons," *Nanotechnology*, vol. 28, no. 6, pp. 065702–065712, 2017.

[11] S. Y. Zhang, L. Li, C. L. Wang, T. F. Zheng, Y. M. Sun, and T. H. Wang, "Preparation of free-standing graphene carbon membrane for gas separation," *CIESC Journal*, vol. 67, no. 10, pp. 4225–4230, 2016.

[12] Z. Qiao, Z. Wang, C. Zhang et al., "PVAm–PIP/PS composite membrane with high performance for CO_2/N_2 separation," *AICHE Journal*, vol. 59, no. 1, pp. 215–228, 2013.

[13] D. Tzeli, G. Theodorakopoulos, I. D. Petsalakis, D. Ajami, and J. Rebek, "Theoretical study of hydrogen bonding in homodimers and heterodimers of amide, boronic acid, and carboxylic acid, free and in encapsulation complexes," *Journal of the American Chemical Society*, vol. 133, no. 42, pp. 16977–16985, 2011.

[14] H. Wang, W. Wang, Y. Zhao et al., "Superior adsorption of 3D nanoporous architectures for Ni(II) ions adsorption using polyvinyl alcohol as cross-linking agent and adsorption conveyor," *RSC Advances*, vol. 8, no. 15, pp. 7899–7903, 2018.

[15] H. Bux, F. Liang, Y. Li, J. Cravillon, M. Wiebcke, and J. Caro, "Zeolitic Imidazolate framework membrane with molecular sieving properties by microwave-assisted solvothermal synthesis," *Journal of the American Chemical Society*, vol. 131, no. 44, pp. 16000-16001, 2009.

[16] R. L. Burns and W. J. Koros, "Defining the challenges for C_3H_6/C_3H_8 separation using polymeric membranes," *Journal of Membrane Science*, vol. 211, no. 2, pp. 299–309, 2003.

[17] L. Jiang, C. Li, H. Yu, Z. Zou, F. Shen, and X. Hou, "Preparation of NH_2-SH-GO/MWCNTs composite for simultaneous removal of Pb(II), Zn(II) and phenol from aqueous solution," *Desalination and Water Treatment*, vol. 97, pp. 272–284, 2017.

[18] Z. Zhang, J. Du, and H. Z. Zhu, "Study on specific surface area and pore size distribution of sponge and palladium by low temperature nitrogen adsorption method," *Rare Metals*, vol. 35, pp. 411–416, 2011.

[19] X. Ma, S. Williams, X. Wei, J. Kniep, and Y. S. Lin, "Propylene/propane mixture separation characteristics and stability of carbon molecular sieve membranes," *Industrial & Engineering Chemistry Research*, vol. 54, no. 40, pp. 9824–9831, 2015.

[20] F. Tian, A. M. Cerro, A. M. Mosier et al., "Surface and stability characterization of a nanoporous ZIF-8 thin film," *The Journal of Physical Chemistry C*, vol. 118, no. 26, pp. 14449–14456, 2014.

[21] C. Y. Park, B. J. Chang, J. H. Kim, and Y. M. Lee, "UV-cross-linked poly(PEGMA-co-MMA-co-BPMA) membranes: synthesis, characterization, and CO_2/N_2 and CO_2/CO separation," *Journal of Membrane Science*, vol. 587, article 117167, 2019.

[22] M. L. Chua, Y. C. Xiao, and T. S. Chung, "Effects of thermally labile saccharide units on the gas separation performance of highly permeable polyimide membranes," *Journal of Membrane Science*, vol. 415-416, pp. 375–382, 2012.

[23] Á. A. Ramírez-Santos, M. Bozorg, B. Addis, V. Piccialli, C. Castel, and E. Favre, "Optimization of multistage membrane gas separation processes. Example of application to CO_2 capture from blast furnace gas," *Journal of Membrane Science*, vol. 566, pp. 346–366, 2018.

[24] R. Banerjee, A. Phan, B. Wang et al., "High-throughput synthesis of zeolitic imidazolate frameworks and application to CO_2 capture," *Science*, vol. 319, no. 5865, pp. 939–943, 2008.

[25] C. Xiong, T. Li, T. Zhao et al., "Two – step approach of fabrication of three – dimensional reduced graphene oxide – carbon nanotubes – nickel foams hybrid as a binder – free supercapacitor electrode," *Electrochimica Acta*, vol. 217, pp. 9–15, 2016.

[26] C. Staudt-Bickel and W. J. Koros, "Olefin/paraffin gas separations with 6FDA-based polyimide membranes," *Journal of Membrane Science*, vol. 170, no. 2, pp. 205–214, 2000.

[27] R. Rostamian and H. Behnejad, "A comparative adsorption study of sulfamethoxazole onto graphene and graphene oxide nanosheets through equilibrium, kinetic and thermodynamic modeling," *Process Safety and Environmental Protection*, vol. 102, pp. 20–29, 2016.

[28] Y. Liu, X. Cai, and W. Shi, "Free-standing graphene/carbon nanotubes/CuO aerogel paper anode for lithium ion batteries," *Materials Letters*, vol. 172, pp. 72–75, 2016.

[29] P. A. M. Mourao, P. J. M. Carrott, and M. M. L. Ribeiro Carrott, "Application of different equations to adsorption isotherms of phenolic compounds on activated carbons prepared from cork," *Carbon*, vol. 44, no. 12, pp. 2422–2429, 2006.

[30] S. Rani, M. Kumar, R. Kumar, D. Kumar, S. Sharma, and G. Singh, "Characterization and dispersibility of improved thermally stable amide functionalized graphene oxide," *Materials Research Bulletin*, vol. 60, pp. 143–149, 2014.

[31] L.-h. Jiang, Y. G. Liu, G. M. Zeng et al., "Removal of 17β-estradiol by few-layered graphene oxide nanosheets from aqueous solutions: external influence and adsorption mechanism," *Chemical Engineering Journal*, vol. 284, pp. 93–102, 2016.

[32] J.-i. Hayashi, H. Mizuta, M. Yamamoto, K. Kusakabe, S. Morooka, and S.-H. Suh, "Separation of ethane/ethylene and propane/propylene systems with a carbonized BPDA–

pp'ODA polyimide membrane," *Industrial & Engineering Chemistry Research*, vol. 35, no. 11, pp. 4176–4181, 1996.

[33] B. L. Tang, H. Zhang, and R. Zuo, "Surface adsorption and diffusion of GaN films grown by MOVPE," *Journal of Synthetic Crystals*, vol. 5, pp. 19–24, 2017.

[34] O. C. David, D. Gorri, A. Urtiaga, and I. Ortiz, "Mixed gas separation study for the hydrogen recovery from $H_2/CO/N_2/CO_2$ post combustion mixtures using a Matrimid membrane," *Journal of Membrane Science*, vol. 378, no. 1-2, pp. 359–368, 2011.

[35] J. A. Lie, T. Vassbotn, M. B. Hägg, D. Grainger, T. J. Kim, and T. Mejdell, "Optimization of a membrane process for CO_2 capture in the steelmaking industry," *International Journal of Greenhouse Gas Control*, vol. 1, no. 3, pp. 309–317, 2007.

[36] W. H. Chen, S. W. Lin, C. Y. Chen, Y. H. Chi, and Y. L. Lin, "Impact of vacuum operation on hydrogen permeation through a palladium membrane tube," *International Journal of Hydrogen Energy*, vol. 44, no. 28, pp. 14434–14444, 2019.